Development of "GaSb-on-Silicon" metamorphic substrates for optoelectronic device growth

Fatih F. Ince[1], Mega Frost[1], Darryl Shima[1], Thomas J. Rotter[1], Sadhvikas Addamane[2], Chadwick L. Canedy[3], Stephanie Tomasulo[3], Chul Soo Kim[3], William W. Bewley[3], Igor Vurgaftman[3], Jerry R. Meyer[3] and Ganesh Balakrishnan[1,4]

[1] *Center for High Technology Materials, The University of New Mexico, Albuquerque, NM*
[2] *Center for Integrated Nanotechnologies, Sandia National Laboratories, Albuquerque, NM,*
[3] *U.S. Naval Research Laboratory, Washington, DC*
[4] *Electrical and Computer Engineering, The University of New Mexico, Albuquerque, NM*

[a)] Electronic mail: gunny@unm.edu

Abstract

The epitaxial development and characterization of metamorphic "GaSb-on-Silicon" buffers as substrates for antimonide devices is presented. The approach involves the growth of a spontaneously and fully-relaxed GaSb metamorphic buffer in a primary epitaxial reactor, and use of the resulting "GaSb-on-Silicon" wafer to grow subsequent layers in a secondary epitaxial reactor. The buffer growth involves four steps – Silicon substrate preparation for oxide removal, nucleation of AlSb on Silicon, growth of the GaSb buffer and finally capping of the buffer to prevent oxidation. This approach on miscut Silicon substrates leads to a buffer with negligible anti-phase domain density. The growth of this buffer is based on inducing interfacial misfit dislocations between an AlSb nucleation layer and the underlying Silicon substrate, which results in a fully relaxed GaSb buffer. A 1 μm thick GaSb layer buffer grown on Silicon has ~ 10^8 dislocations/cm^2. The complete lack of strain in the epitaxial structure allows subsequent growths to be accurately lattice matched, thus making the approach ideal for use as a substrate. We characterize the GaSb-on-Silicon wafer using high-resolution X-Ray diffraction and transmission electron microscopy. The

concept's feasibility is demonstrated by growing interband cascade light emitting devices on the GaSb-on-Silicon wafer. The performance of the resulting LEDs on Silicon approaches that of counterparts grown lattice matched on GaSb.

I. INTRODUCTION

The monolithic growth of III-V compound semiconductors on Silicon substrates has been pursued for several decades, motivated by the inherent advantages of compound semiconductors in new microprocessor architectures and in Silicon photonics. [1–7] While the primary driver has been to integrate III-V active optical components side by side with complementary silicon metal oxide semiconductor (CMOS) components on a single platform, additional device geometries have emerged that use a silicon substrate to provide improved form factor, functionality, cost effectiveness, and thermal management.[8–13] Current issues relating to the growth of III-Vs on silicon include lattice mismatch, thermal expansion coefficient mismatch, and anti-phase domains.[14,15] Lattice mismatch between the Silicon substrate and most III-Vs leads to high threading dislocation densities in the epilayers, which act as non-radiative recombination centers in optoelectronic devices. Furthermore, the mismatch of thermal expansion coefficients leads to micro-cracking in the material when it is thermally cycled or cooled from the growth temperature to room temperature. Finally, antiphase domains with conductive domain walls can form when a polar III-V is grown on non-polar Silicon, which may short diodes and other devices. However, the successful mitigation of these issues should allow III-Vs on Silicon to become a viable commercial technology for electronics and optoelectronics.

One of the earliest demonstrations of a III-V device on silicon was a GaSb-based optically-pumped double heterostructure (DHS) laser.[16,17] Van der Ziel *et al.* showed that GaSb-based metamorphic buffers could be growth on Silicon with relative ease, and that the resulting lasers, while degraded compared to lattice-matched growth, were functional. In later years, several other teams, including Huffaker *et al.* and Tourné *et al.*, demonstrated a variety of antimonide lasers on silicon.[8,18–23] Antiphase domains were eliminated by growing on Silicon substrates with miscuts ranging from 2 to 6 degrees, an approach that similarly yielded a variety of successful polar on non-polar growths such as GaAs on Germanium.[24,25] The mismatch of thermal expansion coefficients has not played a significant role due to the relatively low growth temperature of the antimonide epilayers compared to arsenide- and phosphide-based compound semiconductors. The densities of residual threading dislocations in the antimonide buffers on Silicon have been reported in the $7x10^7/cm^2$ to $1x10^9/cm^2$ range, depending on the thickness of the buffer.[21] A dislocation density of $\approx 5x10^7/cm^2$ is suitable for optoelectronic emitters including light emitting diodes and lasers, although for detectors a further order-of-magnitude reduction is desired.[26]

The highly mismatched growth of GaSb or AlSb on silicon is accomplished by forming periodic misfit dislocations at the III-V/Silicon interface, a growth mode that is unique to the antimonide system. More typically, the mismatched III-V growth follows a pseudomorphic phase and the subsequent formation of misfit dislocations beyond a critical thickness.[27–29] The dislocations then thread into the epi-layer for further relaxation of the metamorphic buffer. Although the initial onset of relaxation is rapid, once the buffer thickness reaches several hundred nanometers the residual relaxation is 70 – 80%.

Several additional microns of growth are then required to complete the relaxation.[30] Since it is impractical to grow beyond 2-3 μm in most cases, the epitaxial process is stopped and the buffer remains only partially relaxed. This makes it challenging to achieve repetitive device results, since the relaxation varies from growth to growth.

Fortunately, antimonides grown on Silicon can bypass the pseudomorpic and partial metamorphic stages. Using certain growth parameters, the antimonide buffer spontaneously undergoes nearly 100% relaxation within a few monolayers of epitaxy. This process does not completely eliminate threading dislocations because the misfit dislocations resulting from the spontaneous relaxation are a mixture of 90-degree and 60-degree types. While the 90-degree Lomer dislocations are stable, the 60-degree dislocations thread into the epilayers. However, the combination of fully relaxed growth with no strain, low growth temperature that reduces thermal stress, and the lower threading dislocation density in interfacial misfit dislocation arrays makes the growth of GaSb on Silicon highly suitable for devices.

In this paper, we demonstrate a process for growing high-quality GaSb based buffers on Silicon substrates in an MBE reactor, which are then transferred to a secondary reactor for device growth. This approach produces "GaSb-on-Silicon" substrates that can replace traditional GaSb substrates in a variety of applications. Transmission electron microscopy (TEM) will be shown that characterizes the optimized growth of GaSb on Silicon. We analyze relaxation in the buffer by high resolution X-Ray diffraction (XRD). Results are then presented showing the experimental characterization of interband cascade light emitting devices (ICLEDs) realized on the GaSb-on-Silicon wafers. The buffers on Silicon were developed at the University of New Mexico, and

then transferred to the Naval Research Laboratory for growth of the ICLEDs. While details of the ICLED growth on silicon and performance of the processed devices can be found elsewhere,[31] the results presented below demonstrate the feasibility of our approach.

II. EXPERIMENTAL

The GaSb-on-Silicon wafers for this study were grown in a VEECO ® GEN 10 elemental source molecular beam epitaxy reactor. The antimony source used in the reactor is a valved cracker that converts Sb_4 from a sublimator to Sb_2. The Aluminum and Gallium sources used are two-zone SUMO ® effusion cells.

The X-Ray diffraction data were collected by a Malvern Panalytical X-Ray diffractometer equipped with a Ge (220) 4 bounce monochromator and a double-axis PIXcel 3D detector. A divergence slit of 1/32^o was used to reduce broadening originating from the X-ray source with filament operating at 40mA. An open detector aperture was used for the initial alignment, and the final scan was collected using a 1mm receiving slit to minimize broadening of the diffracted beam coming from the sample.

TEM analysis was performed on a JEOL NEOARM 200CF running at 200kV. The TEM is equipped with dual JEOL 100mm^2 Silicon Drift Detectors (SDD) for Energy Dispersive Spectroscopy (EDS) data collection. Preparations for both cross sectional and plan view TEM samples were completed on a Thermo Fisher Helios 650 Nanolab system, using standard Focused Ion Beam (FIB) miller based techniques.

A. Preparation of the Silicon substrate for antimonide epitaxy

Removal of the naturally occurring Silicon oxide on the Silicon substrate is critical for success of the epitaxial sequence. The maximum substrate temperature for operation in the antimonide MBE reactors is ~ 750^{o}C. Beyond this, the antimony deposited on the cryopanel walls of the reactor tends to melt and flow, which shorts the effusion cell heater windings and pressure gauges. Since thermal oxide removal is not an option with our current epitaxial setup, we used the alternative of etching the Silicon oxide with dilute HF (50%). The sequence of steps involves submerging the Silicon substrate in the dilute HF solution for 10 Seconds, followed by a rinse in de-ionized (DI) water and then a final HF submersion for an additional 10 Seconds. The resulting Silicon surface is hydrophobic due to hydrogen passivation after the etch. This passivation is not very stable when exposed to atmosphere, so the wafer must be introduced to the vacuum chamber almost immediately. Once in the reactor, reflective high energy electron diffraction (RHEED) of the Silicon substrate shows an oxide-free surface reconstruction, indicating it is suitable for epitaxy.

In order to annihilate antiphase domains, the substrate used in this study was Si (100) with a 4^{o} miscut toward [110]. The oxide removal process for the miscut Silicon was the same as that for (100) surfaces. The Silicon substrate in the MBE growth chamber was heated to 650^{o}C, as measured by a pyrometer, then the temperature was reduced to 420^{o}C for the antimonide growth. The epitaxy started with 20ML AlSb, grown at 0.1 ML/sec. Next 1000 nm GaSb was grown, also at 0.1 ML/sec. Due to the lower bandgap of GaSb compared to Si, the heater temperature was adjusted every 10-20 min to maintain the substrate at 420^{o}C.

B. Nucleation of AlSb/GaSb on Silicon

The growth of III-V emitters on Silicon requires an AlSb-based nucleation layer. This is because the immediate growth of GaSb results in islands that do not coalesce, regardless of the growth thickness. On the other hand, AlSb provides a highly planar nucleation layer. Within 20 MLs of AlSb growth, the Silicon surface is completely covered. However, the continued growth of AlSb beyond a maximum thickness of ≈ 50 nm results in a highly undulating surface. This occurs because the lack of aluminum ad-atom mobility at the reduced growth temperature results in significant lattice rotation at the interface. Thus the optimal growth sequence involves nucleating with AlSb, followed by an immediate transition to GaSb. For the buffers used in this study, we deposited 20 MLs of AlSb followed by 1 μm of GaSb. The effect can be seen in figure 1, where in part (a) a 1 μm thick AlSb layer was grown directly on Silicon and in part (b) a 1 μm thick GaSb layer was grown on 20 MLs of AlSb on Silicon. In the first case, relaxation of the AlSb is ~ 97%. However, the omega-2theta scan shows significant broadening of the AlSb layer peak, with a full width at half maximum (FWHM) of ~ 3500 arcseconds. In figure 1(b), the growth of GaSb on 20 MLs of AlSb results in a much narrower FWHM of ~ 350 arcseconds. The intensity of the epilayer diffraction peak relative to the Silicon substrate peak is also significantly higher in figure 1(b) compared to figure 1(a).

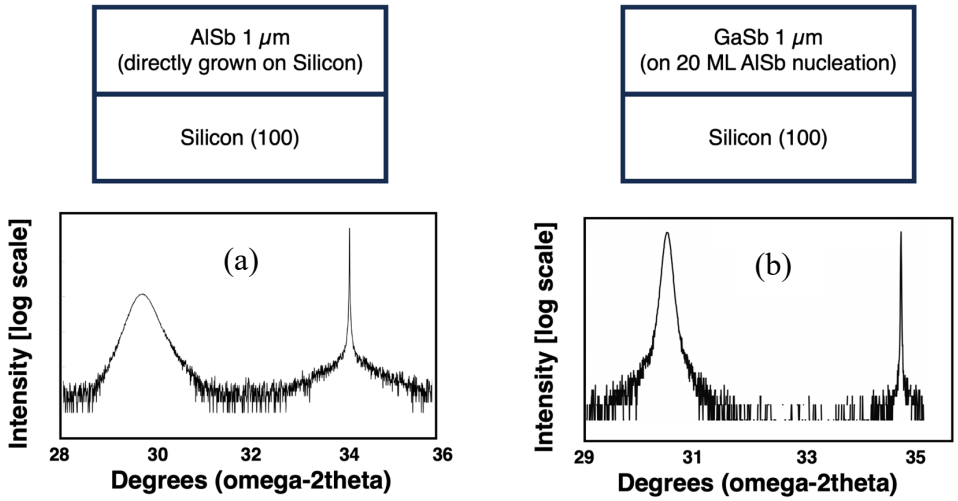

Fig. 1: Epitaxial structure and X-Ray diffraction analysis of (a) 1 μm AlSb grown directly on Silicon and (b) 1 μm GaSb on 20 MLs of AlSb on Silicon.

The transition from growing the AlSb nucleation layer to growth of the highly planar GaSb happens within 100 nm of GaSb epitaxy. This GaSb layer can be grown multiple microns thick with little change to the specular surface morphology.

C. Protective layer of antimony on GaSb-on-Silicon

Typical buffers prepared for optoelectronic device growth are terminated at a GaSb thickness of ≈ 1 μm. This results in ≈ 10^8/cm^2 threading dislocations in the GaSb layer. In the case of miscut substrates, this is also the buffer thickness at which the antiphase domains are no longer discernible. In the initial growths of such buffers, the GaSb epilayer was left exposed to the atmosphere and then transported in a vacuum container to the destination reactor where the epitaxy was performed. However, oxidation of the resulting GaSb surface required a thermal oxide removal process in the destination MBE reactor, which is unsuitable once the GaSb buffer has been grown on Silicon.

Temperatures > 600°C are required because the oxidation does not occur in the controlled environment of a furnace, but instead happens abruptly due to environmental oxygen, which results in non-uniform oxide formation. Consequently, the morphology of GaSb grown on such a surface is very rough. To avoid these issues, we deposit a few monolayers of antimony on the GaSb surface following completion of the initial buffer growth. When done at ~ 250°C, this deposition produces a thin polycrystalline antimony layer on the substrate, as shown in figure 2.

Once the protective layer of antimony is established, the wafer is well encapsulated when exposed to the atmosphere. In the destination reactor, the antimony can be desorbed at a temperature between 400 and 500°C. This is verified using RHEED, with a (1X3) reconstructed GaSb surface emerging as soon as the polycrystalline antimony is desorbed. The process provides a highly planar growth surface that is free of defects and micro-cracks.

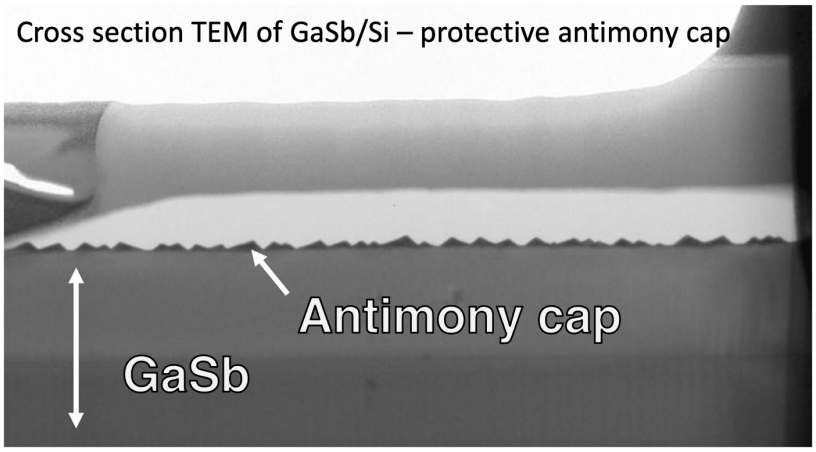

Fig.2: Microscope image of an antimony cap layer that was grown by MBE on the GaSb buffer to protect the surface from oxidation.

III. RESULTS AND DISCUSSION

A. Spontaneous relaxation of the antimonide buffer on Silicon

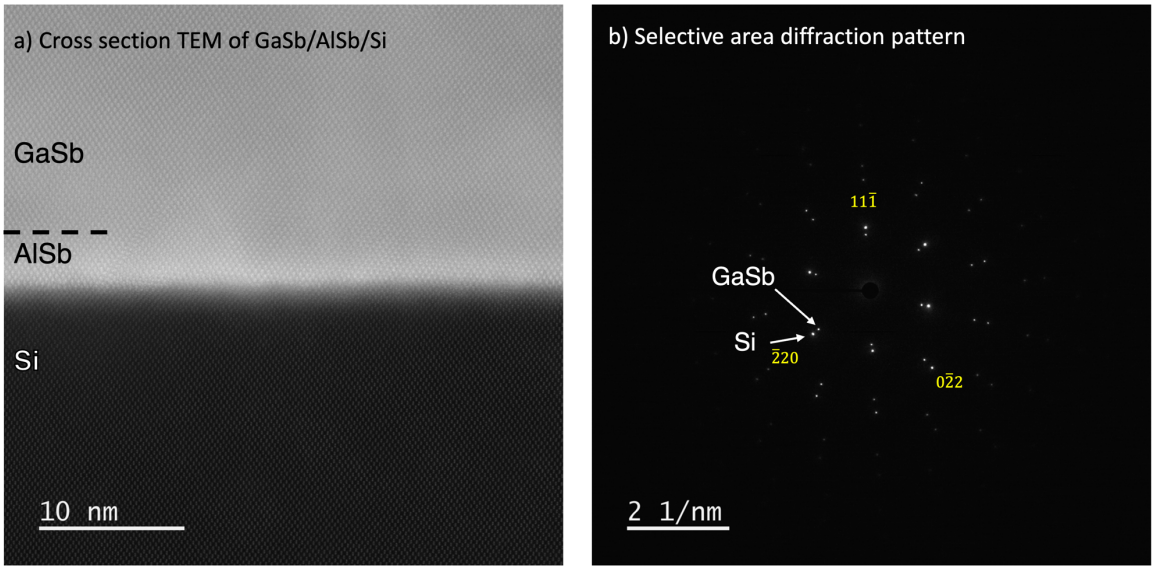

Fig.3: a) TEM cross section of the GaSb/AlSb/Silicon interface, showing atomic resolution of the antimonide layers on Silicon; and b) Selective area diffraction pattern of the III-Sb/Silicon interface, showing two distinct lattice constants.

As mentioned in the introduction, the GaSb buffer growth is fully relaxed across the entire wafer. This phenomenon has been verified on Silicon wafers with up to 3-inch diameter. In figure 3 (left) we observe a high-resolution cross-sectional TEM image of the GaSb/AlSb/Silicon interface grown on a Si (100) substrate with – 4^{o} miscut towards [110]. A Burger's vector analysis of such interfaces shows the presence of both 90^{o} and 60^{o} misfit dislocations. The epilayer is fully relaxed, with no sign of any pseudomorphic phase between the layers and the substrate. The effect was further confirmed by performing selective area diffraction (SAED) of the interface, as shown in figure 3 (right). The pattern clearly indicates the presence of two distinct lattice constants. There

is no evidence for intermediate lattice constants or strain, either of which would manifest as smeared out diffraction spots.

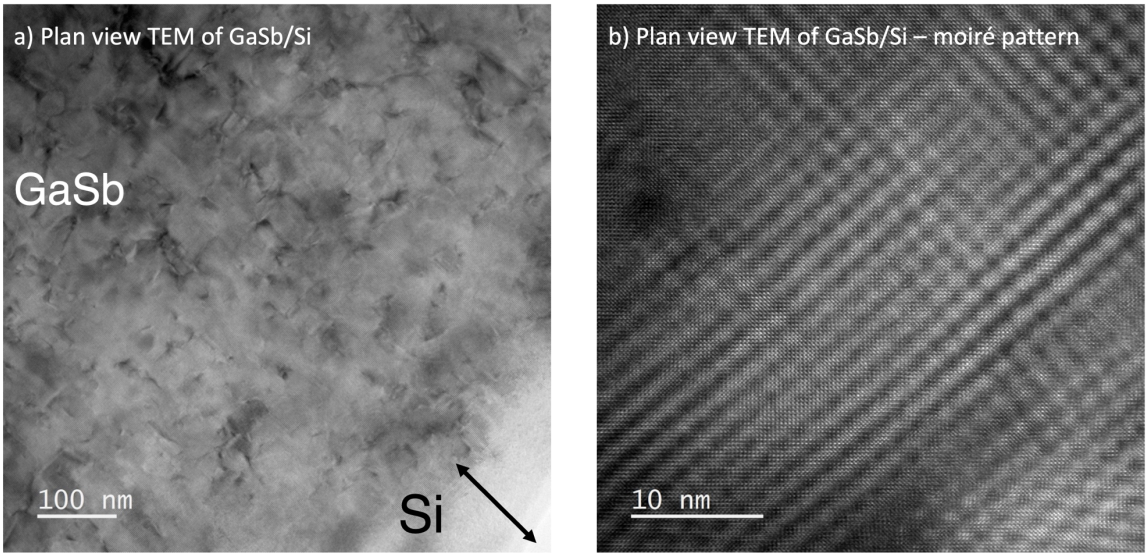

Fig.4 : Plan view TEM image of GaSb/AlSb nucleated on Silicon. In (a) we see the TEM lamella created by tapering of the sample towards the silicon substrate as the sample is thinned into a wedge. In (b) we observe a superimposed moiré pattern over the (100) GaSb surface, which indicates a fully relaxed AlSb/GaSb buffer on Silicon.

A plan view image of the interface was also obtained by milling away most of the epi-layer. This is shown in figure 4 (a), for which a wedge was created to gradually thin the epilayer down to Silicon. Figure 4 (b) shows a higher-resolution image of the same sample. We see a moiré fringe superimposed on the atomic lattice, which results from beating of the two lattice constants and indicates a fully-relaxed antimonide epilayer on Silicon. Analysis of the spacing of the moiré fringe confirms the presence of two distinct lattice constants, at 6.09 and 5.44 Å respectively.

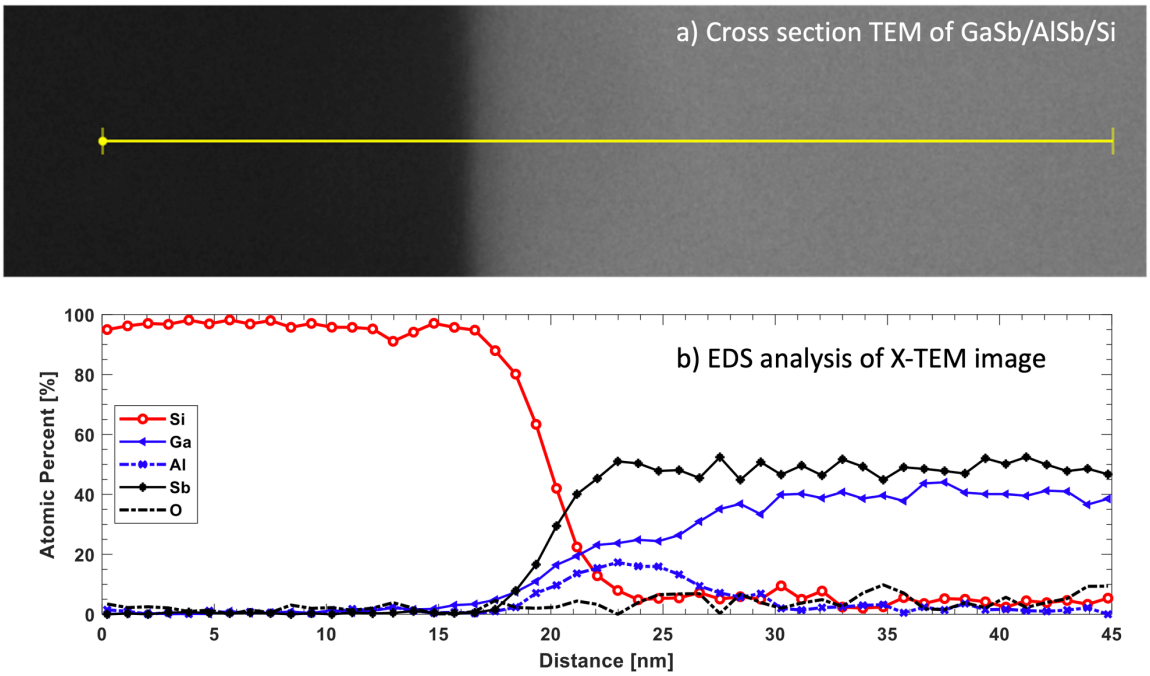

Fig. 5: a) Energy Dispersive Spectroscopy (EDS) line of the GaSb/AlSb/Silicon interface, b)showing the compositional profile.

Figure 5 shows an EDS analysis of the interface. The top section is a TEM image of the GaSb/AlSb/Silicon interface, where the yellow line marks the region over which the EDS analysis was performed. The analysis in the lower section shows the individual layers including the Silicon substrate, the AlSb layer, and the GaSb layer. However, some aspects of this analysis were unexpected. This includes the presence of Silicon for a few nanometers into the AlSb layer, as well as significant intermixing of the AlSb and GaSb layers. We believe that both of these apparent mixing effects occur because the (110) plane is imaged, which means the miscut of the silicon results in a stepped (100) perpendicular to the imaging plane. Thus, the Silicon/AlSb interface gradually changes, moving upwards or downwards as a function of depth. We expect an abrupt interface because there should be negligible Silicon ad-atom movement at the temperatures used to

grow these buffers. The same artefact accounts for the apparent interdiffusion of the AlSb and GaSb layers. The main purpose of this analysis however is to show that the recipe optimization that we have done for the HF-based oxide removal is highly successful. In prior results, we have always observed some oxygen signature from the interface.[32] In this EDS data, there is no interfacial oxygen from oxide remnants at the AlSb/Silicon interface.

B. Residual threading dislocation density

The residual dislocation density in the GaSb layer can be approximated using a High-Resolution X-ray Diffraction (HR-XRD) technique, specifically employing either rocking curve analysis or reciprocal space mapping (RSM). Dislocations in the crystal lattice will broaden the Bragg peak by introducing rotation irregularities and strain fields.[33,34]

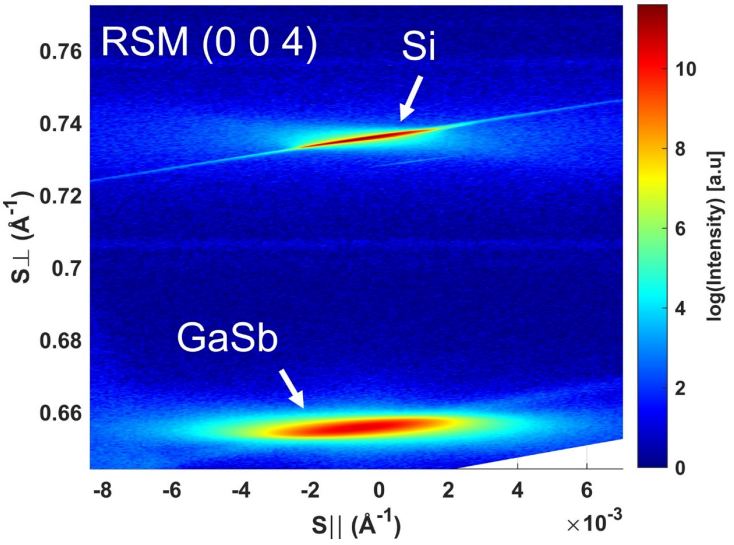

Fig.6: Reciprocal space map based on X-Ray diffraction of a GaSb buffer grown on Silicon (100) with – 4º miscut towards [110]

By combining both symmetrical and asymmetrical RSM scans, we can extract complete information regarding parameters like mosaic spread (microscopic tilt), lateral correlation length, composition, lattice mismatch, residual strain, defect structure, and layer tilt.[35,36]

From an asymmetrical scan (-1 -1 5) of the GaSb buffer, the following formula estimates the dislocation density originating from screw and mixed dislocations:

$$D = \alpha^2/(4.36|b|^2),$$

Here α is the microscopic tilt, or mosaic spread, and |b| is the length of the Burger's vector. Microscopic tilt can be calculated by a graphical analysis, which the following papers explain in greater depth[37–39].

The equation above is solved by integrating the Burger's vector of ($a_{GaSb}/2$) with the microscopic tilt of 178 arcseconds, radians. This yields an estimated residual dislocation density of $2x10^{-8}cm^{-2}$. A similar result is confirmed by TEM.

IV. APPLICATON TO ICLEDs GROWN ON SILICON SUBSTRATES

To demonstrate the growth of antimonide device structures on the GaSb-on-Silicon template, we applied it to ICLEDs grown on silicon.[31] Following preparation of the GaSb/Si wafers at UNM, they were transferred to NRL with an antimony cap. NRL grew the ICLEDs in a RIBER Compact 21T MBE system. The steps included desorption of the antimony cap, growth of an additional 2-3μm-thick GaSb buffer layer, and finally growth of the ICLED with 22 active stages. A control structure was also grown to the same design on a lattice-matched GaSb substrate.

Devices from the best GaSb-on-Silicon wafer displayed performance approaching that of state-of-the-art ICLEDs grown on GaSb.[40] For example, figure 7(a) shows that epi-up ICLEDs grown on silicon exhibited efficiencies 75% of those for epi-down ICLEDs grown on GaSb when architectural differences were accounted for. At 100 mA, 200-µm-diameter mesas produce 184 µW CW at 25°C and 140 µW at 85°C. Due to the much higher thermal conductivity of silicon as compared to GaSb, epi-up ICLEDs on silicon (figure 7(b)) operated to much higher maximum cw output power than ICLEDs grown to the same design on GaSb.

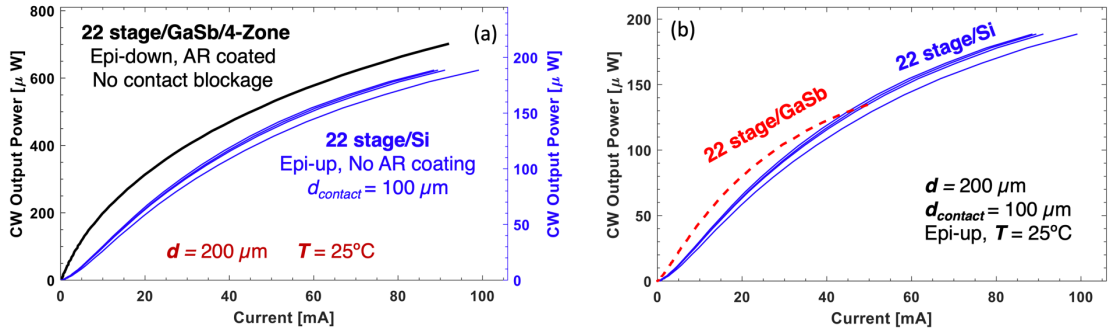

Fig. 7 : (a) Room temperature cw L-I characteristics of multiple epi-up ICLEDs on silicon, compared to that for an epi-down and AR-coated ICLED on GaSb, all with 200 µm mesa diameter. Adjustment of the right power scale by a factor of 3.3 accounts for architectural differences; (b) Cw L-I characteristics at room temperature for multiple 200-µm-diameter ICLEDs on silicon, and for control Wafer grown on GaSb.

V. SUMMARY AND CONCLUSIONS

We have demonstrated GaSb buffers grown on Silicon that provide suitable growth templates for antimonide electronic and optoelectronics devices. We clarified the role played by an AlSb nucleation layer in achieving a single domain and low dislocation

density, with minimal effects due to mismatch of the thermal expansion coefficients. Spontaneous and complete relaxation of the GaSb buffer on the Silicon substrate is confirmed by cross sectional and plan view transmission electron microscopy analyses. An XRD RSM analysis was used to estimate a threading dislocation density of $\approx 10^8/cm^2$ after 1 μm of buffer growth. We also demonstrate that an antimony capping layer on top of the GaSb buffer can protect the surface from oxidation. Proof-of-concept ICLEDs grown on the GaSb-on-Silicon template achieved performance that is at par with lattice-matched devices.

ACKNOWLEDGMENTS

The effort at the University of New Mexico is supported by the U.S.
army research office under contract/grant No. W911NF1910370
and the air force research laboratory under contract/grant No. F19451-22-2-0016.

Electron microscopy was carried out in the Nanomaterials Characterization Facility at the University of New Mexico, a facility that is supported by the State of New Mexico, the National Science Foundation and the National Aeronautics and Space Administration. The acquisition of the JEOL NEOARM AC-STEM at the University of New Mexico was supported by NSF grant DMR-1828731.

This work was performed, in part, at the Center for Integrated Nanotechnologies, an Office of Science User Facility operated for the U.S. Department of Energy (DOE) Office of Science. Sandia National Laboratories is a multimission laboratory managed and operated by National Technology & Engineering Solutions of Sandia, LLC, a wholly owned subsidiary of Honeywell International, Inc., for the U.S. DOE's National Nuclear Security Administration under contract DE-NA-0003525. The views expressed in the article do not necessarily represent the views of the U.S. DOE or the United States Government.

DATA AVAILABILITY

Data underlying the results presented in this paper are not publicly available at this time, but may be obtained from the authors upon reasonable request.

No conflicts of interest

The authors have no conflicts to disclose.

REFERENCES

[1] R. Soref, "Mid-infrared 2 × 2 electro-optical switching by silicon and germanium three-waveguide and four-waveguide directional couplers using free-carrier injection," Photonics Res. **2**(5), 102 (2014).
[2] A. Aiello, D. Das, and P. Bhattacharya, "InGaN/GaN quantum dot light-emitting diodes on silicon with coalesced GaN nanowire buffer layer," ACS Appl. Nano Mater. **4**(2), 1825–1830 (2021).
[3] D.T. Spencer, T. Drake, T.C. Briles, J. Stone, L.C. Sinclair, C. Fredrick, Q. Li, D. Westly, B.R. Ilic, A. Bluestone, N. Volet, T. Komljenovic, L. Chang, S.H. Lee, D.Y. Oh, M.-G. Suh, K.Y. Yang, M.H.P. Pfeiffer, T.J. Kippenberg, E. Norberg, L. Theogarajan, K. Vahala, N.R. Newbury, K. Srinivasan, J.E. Bowers, S.A. Diddams, and S.B. Papp, "An optical-frequency synthesizer using integrated photonics," Nature **557**(7703), 81–85 (2018).
[4] H. Larocque, M.A. Buyukkaya, C. Errando-Herranz, S. Harper, J. Carolan, C.-M. Lee, C.J.K. Richardson, G.L. Leake, D.J. Coleman, M.L. Fanto, E. Waks, and D. Englund, "Tunable quantum emitters on large-scale foundry silicon photonics," ArXiv [Physics.Optics], (2023).
[5] E. Stanton, A. Spott, J. Peters, M. Davenport, A. Malik, N. Volet, J. Liu, C. Merritt, I. Vurgaftman, C. Kim, J. Meyer, and J. Bowers, "Multi-spectral quantum cascade lasers on silicon with integrated multiplexers," Photonics **6**(1), 6 (2019).
[6] J.-H. Kim, S. Aghaeimeibodi, C.J.K. Richardson, R.P. Leavitt, D. Englund, and E. Waks, "Hybrid Integration of Solid-State Quantum Emitters on a Silicon Photonic Chip," Nano Lett. **17**(12), 7394–7400 (2017).
[7] N. Margalit, C. Xiang, S.M. Bowers, A. Bjorlin, R. Blum, and J.E. Bowers, "Perspective on the future of silicon photonics and electronics," Appl. Phys. Lett. **118**(22), 220501 (2021).
[8] Z. Loghmari, J.-B. Rodriguez, A.N. Baranov, M. Rio-Calvo, L. Cerutti, A. Meguekam, M. Bahriz, R. Teissier, and E. Tournié, "InAs-based quantum cascade lasers grown on on-axis (001) silicon substrate," APL Photonics **5**(4), 041302 (2020).
[9] K.D. Maranowski, J.M. Peterson, S.M. Johnson, J.B. Varesi, A.C. Childs, R.E. Bornfreund, A.A. Buell, W.A. Radford, T.J. de Lyon, and J.E. Jensen, "MBE growth of HgCdTe on silicon substrates for large format MWIR focal plane arrays," J. Electron. Mater. **30**(6), 619–622 (2001).
[10] D.C. Bobela, L. Gedvilas, M. Woodhouse, K.A.W. Horowitz, and P.A. Basore, "Economic competitiveness of III–V on silicon tandem one-sun photovoltaic solar modules in favorable future scenarios," Prog. Photovoltaics Res. Appl. **25**(1), 41–48 (2017).
[11] S. Manda, R. Matsumoto, S. Saito, S. Maruyama, H. Minari, T. Hirano, T. Takachi, N. Fujii, Y. Yamamoto, Y. Zaizen, and Others, in *2019 IEEE International Electron Devices Meeting (IEDM)* (IEEE, 2019), pp. 16–17.
[12] K. Sun, D. Jung, C. Shang, A. Liu, J. Morgan, J. Zang, Q. Li, J. Klamkin, J.E. Bowers, and A. Beling, "Low dark current III--V on silicon photodiodes by heteroepitaxy," Opt. Express **26**(10), 13605–13613 (2018).

[13] J.R. Meyer, A. Spott, C.S. Kim, M. Kim, C.L. Canedy, C.D. Merritt, W.W. Bewley, and I. Vurgaftman, "Weak Index Guiding of Interband Cascade Lasers," U. S. Patent Application **18**, (2023).
[14] J.C.C. Fan, and J.M. Poate, editors , *MRS Proceedings Heteroepitaxy on Silicon: Volume 67* (Materials Research Society, 1986).
[15] J.C.C. Fan, J.M. Phillips, and B.-Y. Tsaur, editors , *MRS Proceedings Heteroepitaxy on Silicon II: Volume 91* (Materials Research Society, 1987).
[16] R.J. Malik, J.P. Van Der Ziel, B.F. Levine, C.G. Bethea, and J. Walker, "Molecular-beam epitaxy of GaSb/AlSb optical device layers on Si (100)," J. Appl. Phys. **59**(11), 3909–3911 (1986).
[17] J. van der Ziel, R. Malik, J. Walker, and R. Mikulyak, "Optically pumped laser oscillation in the 1.6 - 1.8 μm region from strained layer Al0.4Ga0.6Sb/GaSb/ Al0.4Ga0.6Sb/Double heterostructures grown by molecular beam hetero-epitaxy on Si substrates," IEEE J. Quantum Electron. **22**(9), 1587–1592 (1986).
[18] A. Remis, L. Monge, G. Boissier, J.-B. Rodriguez, L. Cerutti, and E. Tournié, in *Novel In-Plane Semiconductor Lasers XXI*, edited by A.A. Belyanin and P.M. Smowton (SPIE, 2022).
[19] D.L. Huffaker, G. Balakrishnan, A. Jallipalli, M.N. Kutty, J. Tatebayashi, S.H. Huang, L.R. Dawson, Z. Mi, and P. Bhattacharya, "1.54 μm Monolithically Integrated GaSb Quantum Well Laser Diode on Silicon Operating at 77K," 2007 International Nano-Optoelectronics Workshop, (2007).
[20] A. Jallipalli, M.N. Kutty, G. Balakrishnan, J. Tatebayashi, N. Nuntawong, S.H. Huang, L.R. Dawson, D.L. Huffaker, Z. Mi, and P. Bhattacharya, "1.54 μm GaSb/AlGaSb multi-quantum-well monolithic laser at 77 K grown on miscut Si substrate using interfacial misfit arrays," Electron. Lett. **43**(22), 1198–1199 (2007).
[21] J. Tatebayashi, A. Jallipalli, M.N. Kutty, S. Huang, K. Nunna, G. Balakrishnan, L.R. Dawson, and D.L. Huffaker, "Monolithically Integrated III-Sb-Based Laser Diodes Grown on Miscut Si Substrates," IEEE J. Sel. Top. Quantum Electron. **15**(3), 716–723 (2009).
[22] J.B. Rodriguez, L. Cerutti, G. Patriarche, L. Largeau, K. Madiomanana, and E. Tournié, "Characterization of antimonide based material grown by molecular epitaxy on vicinal silicon substrates via a low temperature AlSb nucleation layer," J. Cryst. Growth **477**, 65–71 (2017).
[23] L. Cerutti, D.A. Díaz Thomas, J.-B. Rodriguez, M. Rio Calvo, G. Patriarche, A.N. Baranov, and E. Tournié, "Quantum well interband semiconductor lasers highly tolerant to dislocations," Optica **8**(11), 1397 (2021).
[24] S.M. Ting, and E. Fitzgerald, "Metal-organic chemical vapor deposition of single domain GaAs on Ge/Ge x Si 1- x/Si and Ge substrates," J. Appl. Phys. **87**(5), 2618–2628 (2000).
[25] S. Strite, D. Biswas, N.S. Kumar, M. Fradkin, and H. Morkoc, "Antiphase domain free growth of GaAs on Ge in GaAs/Ge/GaAs heterostructures," Appl. Phys. Lett. **56**(3), 244–246 (1990).
[26] E. Plis, J.B. Rodriguez, G. Balakrishnan, Y.D. Sharma, H.S. Kim, T. Rotter, and S. Krishna, "Mid-infrared InAs/GaSb strained layer superlattice detectors with nBn design grown on a GaAs substrate," Semicond. Sci. Technol. **25**(8), 085010 (2010).

[27] R. People, and J.C. Bean, "Calculation of critical layer thickness versus lattice mismatch for GexSi1−x/Si strained-layer heterostructures," Appl. Phys. Lett. **47**(3), 322–324 (1985).
[28] J.W. Matthews, A.E. Blakeslee, and S. Mader, "Use of misfit strain to remove dislocations from epitaxial thin films," Thin Solid Films **33**(2), 253–266 (1976).
[29] J.W. Matthews, and A.E. Blakeslee, "Defects in epitaxial multilayers: I. Misfit dislocations," J. Cryst. Growth **27**, 118–125 (1974).
[30] W. Qian, M. Skowronski, and R. Kaspi, "Dislocation Density Reduction in GaSb Films Grown on GaAs Substrates by Molecular Beam Epitaxy," J. Electrochem. Soc. **144**(4), 1430 (1997).
[31] C.L. Canedy, W.W. Bewley, S. Tomasulo, C.S. Kim, C.D. Merritt, I. Vurgaftman, J.R. Meyer, M. Kim, T.J. Rotter, G. Balakrishnan, and T.D. Golding, "Mid-infrared interband cascade light emitting devices grown on off-axis silicon substrates," Opt. Express **29**(22), 35426–35441 (2021).
[32] G. Balakrishnan, S. Huang, L.R. Dawson, Y.-C. Xin, P. Conlin, and D.L. Huffaker, "Growth mechanisms of highly mismatched AlSb on a Si substrate," Appl. Phys. Lett. **86**(3), 034105 (2005).
[33] J.E. Ayers, "The measurement of threading dislocation densities in semiconductor crystals by X-ray diffraction," J. Cryst. Growth **135**(1–2), 71–77 (1994).
[34] D. Benyahia, Ł. Kubiszyn, K. Michalczewski, A. Kębłowski, P. Martyniuk, J. Piotrowski, and A. Rogalski, "Interfacial misfit array technique for GaSb growth on GaAs (001) substrate by molecular beam epitaxy," J. Electron. Mater. **47**(1), 299–304 (2018).
[35] A. Authier, in *X-Ray and Neutron Dynamical Diffraction* (Springer US, Boston, MA, 1996), pp. 1–31.
[36] M. Frentrup, L.Y. Lee, S.-L. Sahonta, M.J. Kappers, F. Massabuau, P. Gupta, R.A. Oliver, C.J. Humphreys, and D.J. Wallis, "X-ray diffraction analysis of cubic zincblende III-nitrides," J. Phys. D Appl. Phys. **50**(43), 433002 (2017).
[37] F.F. Ince, M. Frost, S. Seth, D. Shima, T.J. Rotter, and G. Balakrishnan, "MBE growth of In0.53Ga0.47Sb on In0.53Ga0.47As/InP substrates using the interfacial misfit dislocation arrays," J. Vac. Sci. Technol. A **41**(5), (2023).
[38] M. Polat, O. Arı, O. Öztürk, and Y. Selamet, "Reciprocal space mapping study of CdTe epilayer grown by molecular beam epitaxy on (2 1 1)B GaAs substrate," Mater. Res. Express **4**(3), 035904 (2017).
[39] M.A. Moram, and M.E. Vickers, "X-ray diffraction of III-nitrides," Rep. Prog. Phys. **72**(3), 036502 (2009).
[40] C.S. Kim, W.W. Bewley, C.D. Merritt, C.L. Canedy, M.V. Warren, I. Vurgaftman, J.R. Meyer, and M. Kim, "Improved mid-infrared interband cascade light-emitting devices," Organ. Ethic. **57**(1), 011002 (2017).